Hindawi Publishing Corporation
Journal of Nanomaterials
Volume 2014, Article ID 340384, 6 pages
http://dx.doi.org/10.1155/2014/340384

*Research Article*

# Vibrational Order, Structural Properties, and Optical Gap of ZnO Nanostructures Sintered through Thermal Decomposition

**Alejandra Londono-Calderon, Fernando F. Jurado-Lasso, Juan D. Romero-Salazar, Nathaly Jurado-Lasso, and J. Fabian Jurado**

*Laboratorio de Propiedades Térmicas Dieléctricas de Compositos, Departamento de Física y Química, Universidad Nacional de Colombia, A.A. 127, Manizales, Colombia*

Correspondence should be addressed to J. Fabian Jurado; jfjurado@unal.edu.co

Received 6 June 2014; Revised 15 August 2014; Accepted 15 August 2014; Published 15 September 2014

Academic Editor: Shadi A. Dayeh



The sintering of different ZnO nanostructures by the thermal decomposition of zinc acetate is reported. Morphological changes from nanorods to nanoparticles are exhibited with the increase of the decomposition temperature from 300 to 500°C. The material showed a loss in the crystalline order with the increase in the temperature, which is correlated to the loss of oxygen due to the low heating rate used. Nanoparticles have a greater vibrational freedom than nanorods which is demonstrated in the rise of the main Raman mode $E_2$ (high) during the transformation. The energy band gap of the nanostructured material is lower than the ZnO bulk material and decreases with the rise in the temperature.

## 1. Introduction

Zinc oxide is one of the most promising semiconductors of group II–VI for manufacturing technological devices on a nanometric scale. Since the surface/volume ratio in nanostructures is higher than in bulk materials, the quantum effects dominate the properties. The precise control between morphology and the desired properties has been used in the study and fabrication of gas nanosensors [1–3], light emitting diodes [4], solar cells [5–7], field effect transistors [8], and in photocatalysts [9–11] among others [12]. Throughout the pursuit of these objectives, a wide diversity of sintering techniques have been implemented. Lower cost methodologies, such as thermal decomposition, are the ones positioned in the first place. The thermal decomposition method is an endothermic process where heat is used to break the links within the initial precursor in order to obtain one or more final components. It has been found that this technique allows the growth of nanoparticles [13–16], nanowires, and nanorods [17–19] among others [20]. Zinc acetate decomposes into zinc oxide when being subjected to thermal treatments, generally above 200°C. This methodology provides an advantage compared to other methods due to the simplicity and the fact that it does not require reducing or additive agents. To obtain zinc oxide through thermal decomposition, some methodologies have reported results as a function of the decomposition temperature, time, and the aging [16, 19, 21–24]. However the relationship between morphology, structural, vibrational, and optical properties and the decomposition process is still not clear. In this work, ZnO nanostructures have been sintered from the thermal decomposition of zinc acetate at three different temperatures (300, 400, and 500°C) for a low heating rate and a long annealing time. The morphological, structural, vibrational, and material optical gap variations are being studied.

## 2. Experimental Details

The sinterization of ZnO nanostructures is as follows: 0.5 g of zinc acetate dihydrate ($Zn(CH_3COO)_2 \cdot 2H_2O$ Sigma Aldrich 98+%) is ground in a mortar for 5 minutes; the powdered material is placed in a crucible, which is inserted in a programmable furnace and heated at a rate of 100°C/h to a temperature of 300, 400, and 500°C for a period of 24 hours. The final product is approximately 0.15 g of ZnO, which is

stored within a controlled environment for its respective characterization.

The structural characterization was carried out by using a Bruker D8 Advance X-Ray diffractometer (radiation of $CuK_\alpha$, $\lambda$ = 1,5406 Å); the vibrational order was assessed through Raman microscopy by using $\mu$-Raman Confocal LabRam HR Horiba Jobin Yvon equipment with a monochromatic laser source of 473 nm. The optical gap was established from absorption by using a UV/Vis Perkin Elmer Lambda 20 spectrophotometer. The morphology was identified by the use of a Transmission Electron Microscope (TEM) JEOL 2010-F working at 200 kV and a Scanning Electron Microscope (SEM) Hitachi 5500 at 30 kV.

The change of the morphology of ZnO sintered by thermal decomposition of zinc acetate has already been reported [22–24]. Farbod and Jafarpoor [22] report an increase in oxygen deficiency with the annealing time and the final color of the sample. Each increment of the temperature leads to an increase in the total sinter time; for 500°C the long heating time (5 hours) may be responsible for a oxygen deficiency in the final sample. This is also related to the color of the powder which changes from white at 300°C to pale yellow at 500°C.

## 3. Results and Discussion

The thermodynamic mechanism of the zinc acetate decomposition into ZnO is well known. Initially, the loss of 2 water molecules is observed. The anhydrous acetate reacts with water in the environment to form a basic zinc acetate and acetic acid $CH_3COOH$. In the decomposition of zinc complex, 4ZnO molecules, acetate $CH_3COCH_3$, and carbon dioxide $CO_2$ are produced [18, 25]. The reaction is as follows:

$$\begin{aligned} \mathrm{Zn(CH_3COO)_2 \cdot 2H_2O} &\longrightarrow \mathrm{Zn(CH_3COO)_2 + 2H_2O} \uparrow \\ \mathrm{4Zn(CH_3COO)_2 + 2H_2O} &\longrightarrow \mathrm{Zn_4O(CH_3COO)_6} \\ &\quad + \mathrm{2CH_3COOH} \uparrow \\ \mathrm{Zn_4O(CH_3COO)_6} &\longrightarrow \mathrm{4ZnO + 3CH_3COCH_3} \uparrow \\ &\quad + \mathrm{3CO_2} \uparrow \end{aligned} \tag{1}$$

The variation in the properties of the ZnO during this process must be correlated to the combination of decomposition temperature, heating rate, and time used for the experiment. For our case of study, Figure 1 shows TEM and SEM images of the material obtained at a fixed heating rate at a temperature of (a–d) 300, (e–h) 400, and (i–l) 500°C. The sample sintered at 300°C is mainly formed by nanorod structures with an average diameter of 35 ± 10 nm and an average length of 400 ± 196 nm. The preferential growth of the nanorods is in the (0001) direction. A high dispersion in the size of the nanorods is observed (inset Figures 1(a) and 1(b)). A low heating rate produces a more achievable loss of water molecules, which are essential in the decomposition process of the zinc acetate [22]. During the formation of hexagonal ZnO, the polar faces (0001) are unstable and have a faster growth rate than the nonpolar faces. By the time the temperature has reached the 300°C there is a lack of nucleation sites, and the long period of time of the annealing promotes then the growth of rod-like structures orientated along the *c* axis.

Table 1: Lattices parameters and crystallite size.

| Temperature (°C) | *a* (Å) | *c* (Å) | *D* (Å) |
|---|---|---|---|
| 300 | 3.247 | 5.202 | 247 ± 21 |
| 400 | 3.252 | 5.212 | 180 ± 11 |
| 500 | 3.254 | 5.210 | 195 ± 9 |

For the sample collected at 400°C a change in the morphology is observed. The resulting nanostructures are a combination of nanorods and nanoparticles. The average sizes of the nanoparticles are 48 ± 13 nm (inset Figure 1(g)) whereas the nanorods have an average diameter of 34 ± 9 nm with an average length of 332 ± 88 nm (inset Figures 1(e)-1(f)). Once the temperature has increased to 500°C, hexagonal-like nanoparticles of 104 ± 22 nm are observed (inset Figure 1(i)). A higher temperature creates more nucleation sites of which nanoparticles can start to grow, producing a higher consumption of the precursor, favoring a homogeneous growth in all the directions of the hexagonal structure and lead the transformation from nanorods to nanoparticles.

*3.1. Structure.* Figure 2 shows the XRD diffractograms for the treated material at 300, 400, and 500°C, respectively. All the diffraction peaks correspond to the hexagonal phase of the ZnO according to JCPDS card number 36–1451; no impurity peaks were detected. The lattice parameters were established through the Cohen method and the mean crystallite size (*D*) was determined by the use of Scherrer's equation:

$$D = \frac{0.9\lambda}{\beta \cos\theta}, \tag{2}$$

where $\lambda$ is the wavelength of the X-ray radiation and $\beta$ is the full width at half maximum (FWHM) of each diffraction peak. The different values for *D* and the lattice parameters are presented in Table 1.

It is observed that the temperature has an influence on crystallite domain size. Narrow peaks are present in the 300°C sample in which the crystallite size is comparable to the diameter of the nanorods. This may imply that the nanorods are formed by groups of crystallite pilled-up along the growth axis *c*. An increment in the FWHM value and a decrease in the relative intensity of the peaks are observed for the higher temperature of 500°C. At this temperature there are more nucleation sites that allow the growth of nanoparticles formed by random arrangements of smaller crystallites. Increasing the temperature does not promote grain boundary diffusion; as a result a loss in the crystalline order is observed. ZnO has a tendency to lose oxygen [26], during the heating time before reaching the annealing temperature of 500°C in which more water escapes from the furnace and it is more likely to obtain a nonstoichiometric material.

*3.2. Micro-Raman.* Figure 3 shows the micro-Raman spectra results of the obtained materials as well as the ZnO reference.

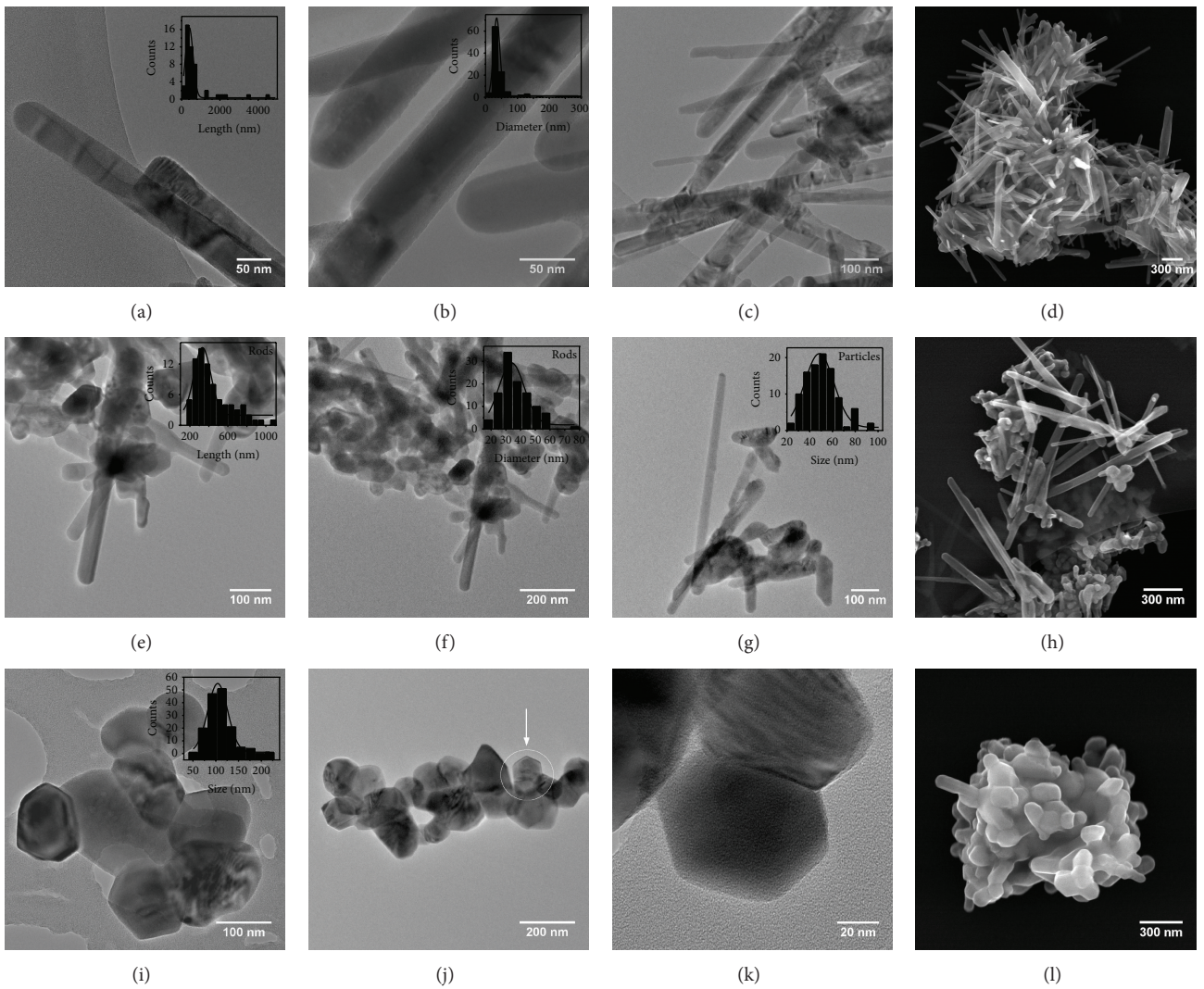


Figure 1: TEM and SEM images of ZnO samples fabricated at (a–d) 300°C, (e–h) 400°C, and (i–l) 500°C. The insets on (a, b, e–g, and i) represent the size distribution of the structures. The arrow in (j) shows a hexagonal-like crystal present in the sample at 500°C.

Table 2: ZnO vibrational modes and relative intensity of the bands.

| Mode | Reference | | 300°C | | 400°C | | 500°C | |
|---|---|---|---|---|---|---|---|---|
| | Wavelength | $I_i/I_0$ ($cm^{-1}$) | Wavelength | $I_i/I_0$ ($cm^{-1}$) | Wavelength | $I_i/I_0$ ($cm^{-1}$) | Wavelength | $I_i/I_0$ ($cm^{-1}$) |
| $E_{2H} - E_{2L}$ | 328 | 26.5 | 327 | 51.5 | 331 | 26.9 | 332 | 15.5 |
| $A_1$ (TO) | 376 | 57.8 | 386 | 15.9 | 390 | 7.30 | 387 | 6.10 |
| $E_1$ (TO) | 410 | 19.4 | 428 | 24.1 | 431 | 14.9 | 434 | 30.0 |
| $E_2$ (high) | 437 | 100 | 436 | 100 | 439 | 100 | 439 | 100 |
| $E_{2H} + E_{2L}$ | 536 | 4.50 | 528 | 4.50 | 533 | 10.3 | 538 | 3.50 |
| $A_1$ (LO) | — | — | 573 | 20.7 | 572 | 7.60 | 573 | 3.80 |
| $E_1$ (LO) | — | — | — | — | 583 | 4.70 | 585 | 3.80 |

All the vibrational modes correspond to the ones predicted by the theory and experiments reported in the literature [25, 27–29]. Table 2 presents the vibrational peaks and the respective percentage of relative intensity ($I_i/I_0$), where $I_0$ is the intensity of the most intense and characteristic band $E_2$(high) antisymmetric, which is related to oxygen attached to zinc atoms in the tetrahedral configuration. Longitudinal optical modes $A_1$(LO) and $E_1$(LO) are not evident in the obtained material, since they are only visible when the axis $c$ of the wurtzite structure is parallel to the surface. For

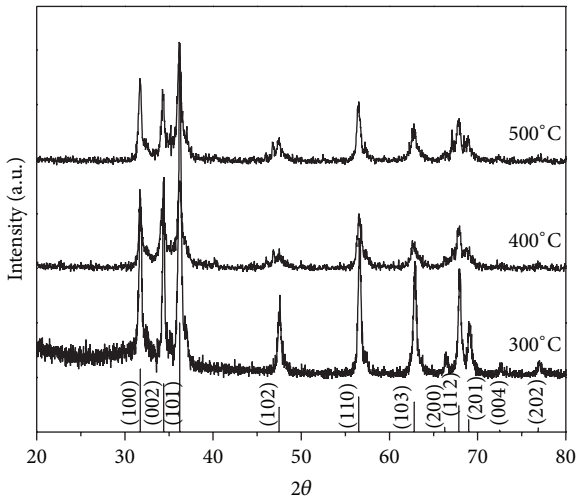


FIGURE 2: XRD diffractogram of ZnO nanostructure samples fabricated at 300, 400, and 500°C, respectively. This growth can be observed from the presence of the peaks at 31.76, 34.32, 36.22, 47.56, 56.58, 62.84, 66.44, 68.04, 69.12, 72.7, and 76.94 which correspond to (100), (002), (101), (102), (110), (103), (200), (112), (201), (004), and (202) orientations, respectively. As shown in the XRD data, the (101) direction is the preferred orientation for the three samples. Reference corresponds to JCPDS card number 36-1451.

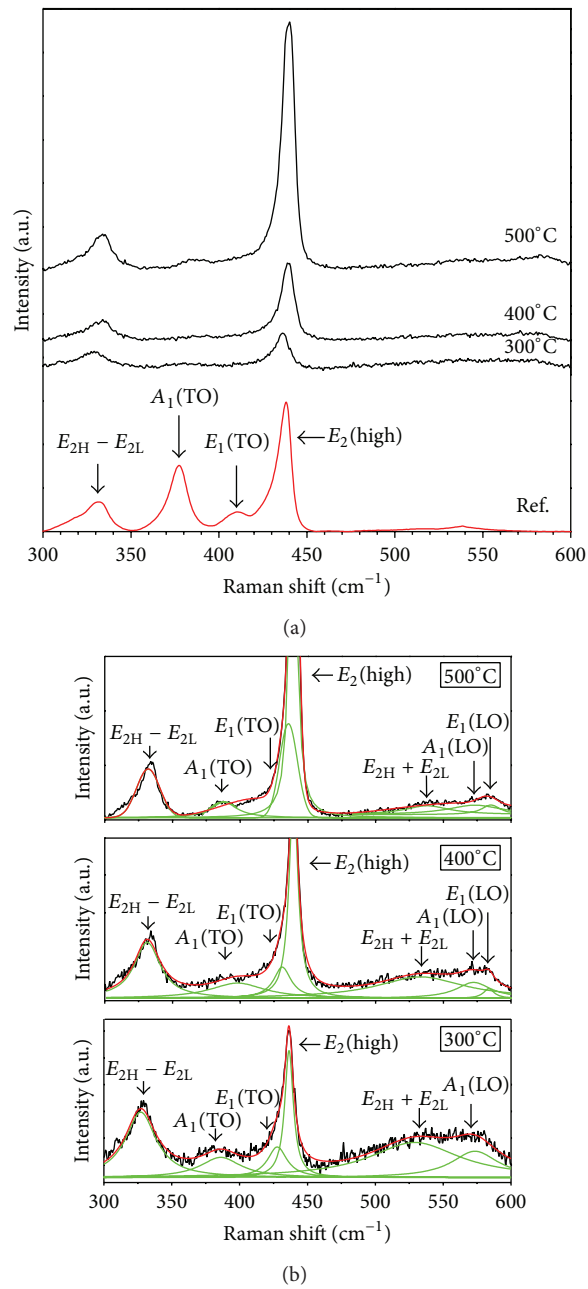


FIGURE 3: (a) Raman spectra of ZnO samples fabricated at 300, 400, and 500°C, respectively, and reference. (b) Raman spectra at room temperature of ZnO samples fabricated at 300, 400, and 500°C, respectively. ZnO phonon modes as well as molecular vibrations are observed for comparison, and the spectrum of ZnO reference is shown.

the nanostructured material there are no constraints for the longitudinal optical modes due to the fact that the structures are randomly organized.

The bands located between the interval of 327 to 332 cm$^{-1}$ and 528 to 538 cm$^{-1}$ correspond to the multiphononic modes of second order, which are expressed with [$E_2$(high) − $E_2$(low)] and [$E_2$(high) + $E_2$(low)], respectively and do not differ from other reports.

The nanorod morphology constrains the vibrational degrees of freedom of the molecules. The nanoparticle morphology allows a greater freedom in the vibration of the characteristic mode $E_2$(high). The $A_1$ longitudinal and transversal modes are associated to parallel displacement of oxygen atoms on the $c$ axis and are more intense for the 300°C sample since the structure is preferentially oriented in this direction. As a result of the increase in the temperature, the $A_1$ modes decrease due to the oxygen deficiency. In addition, the presence of the mode $E_1$(LO) is more prominent with the increase in the temperature which is related to an oxygen deficiency [29–31].

*3.3. Optical Absorption.* Figure 4(a) shows the absorbance spectrum as a function of the wavelength for the sintered materials at 300, 400, and 500°C. From these results, the forbidden energy band $E_g$ is established according to Tauc's expression:

$$Ah\nu = B\left(h\nu - E_g\right)^m, \tag{3}$$

where $A$ is the absorption, $B$ is a constant, and $m$ is taken as 1/2 for direct-gap materials. From the dependence of $(Ah\nu)^2$ with the energy (Figure 4(b)) the energy gap in the material is obtained. The energies determined for the materials were 3.21 ± 0.04, 3.20 ± 0.07, and 3.17 ± 0.03 eV for 300, 400, and 500°C, respectively.

A small decrease in the $E_g$ value with the increase in the temperature is observed. The values hereby reported are lower than the one for the bulk material of 3.37 eV. This is opposite to the expected outcome for nanostructures and it may be due to the presence of defects and impurity levels

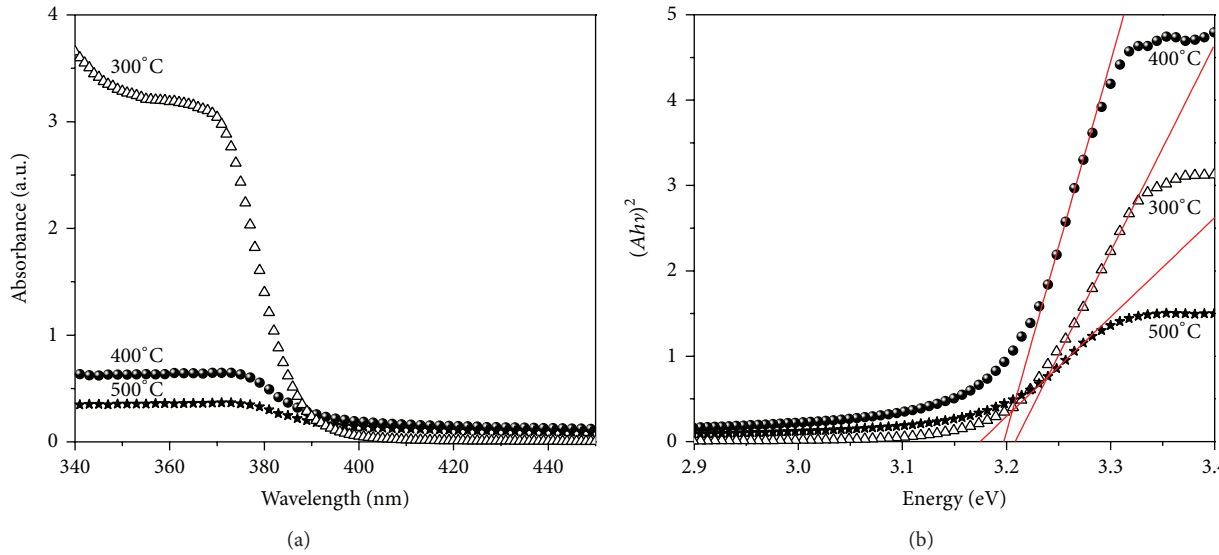


FIGURE 4: (a) Absorbance spectrum of ZnO sintered at 300, 400, and 500°C, respectively. (b) $(Ahν)^2$ versus energy. The solid lines represent the linear fit.

inside the band gap and is in good agreement with other reports [16, 21, 22, 32].

## 4. Conclusions

The thermal decomposition of zinc acetate allows the production of ZnO nanorods at 300°C and hexagonal-like nanoparticles at 500°C. Increasing temperatures favor the homogeneous crystallization among the different polar and nonpolar planes, as well as promoting the morphological transformation from nanorods to nanoparticles. A higher temperature creates more nucleation sites in which nanoparticles can start to grow. The slow heating rate is responsible for the loss of water and the oxygen deficiency rise. The average diameter of the nanorods is comparable to the crystallite size. Increments in the temperature reduce the size of the crystalline domains. The sintered material at 300°C shows a better crystalline organization in comparison to the obtained material at 400 and 500°C. The rise of the temperature increases the presence of structural defects, which are demonstrated with the increase of Raman mode $E_1$(LO) and the reduction of the $A_1$ modes, related to the presence of oxygen vacancies. The energy band gap decreases with the temperature and in all the cases is lower than the bulk value.

## Conflict of Interests

The authors declare that there is no conflict of interests regarding the publication of this paper.

## Acknowledgments

This work was carried out with the support of the Research Information System HERMES from the National University of Colombia, Project no. 15875. The authors wish to thank the plasma physics, material optical properties, and nanostructured and functional materials laboratories from The National University of Colombia-Manizales for the XRD, Raman, and UV-Vis measurements. The authors wish to thank as well the University of Texas at San Antonio and The Kleberg Advanced Microscopy Laboratory where the TEM and SEM measurements were carried out.

## References

[1] O. Lupan, G. A. Emelchenko, V. V. Ursaki et al., "Synthesis and characterization of ZnO nanowires for nanosensor applications," *Materials Research Bulletin*, vol. 45, no. 8, pp. 1026–1032, 2010.

[2] K.-M. Kim, H.-R. Kim, K.-I. Choi, H.-J. Kim, and J.-H. Lee, "ZnO hierarchical nanostructures grown at room temperature and their $C_2H_5OH$ sensor applications," *Sensors and Actuators B: Chemical*, vol. 155, no. 2, pp. 745–751, 2011.

[3] M. M. Arafat, B. Dinan, S. A. Akbar, and A. S. M. A. Haseeb, "Gas sensors based on one dimensional nanostructured metal-oxides: a review," *Sensors*, vol. 12, no. 6, pp. 7207–7258, 2012.

[4] P. C. Tao, Q. Feng, J. Jiang et al., "Electroluminescence from ZnO nanowires homojunction LED grown on Si substrate by simple chemical vapor deposition," *Chemical Physics Letters*, vol. 522, pp. 92–95, 2012.

[5] C. Luan, A. Vaneski, A. S. Susha et al., "Facile solution growth of vertically aligned ZnO nanorods sensitized with aqueous CdS and CdS equantum dots for photovoltaic applications," *Nanoscale Research Letters*, vol. 6, p. 340, 2011.

[6] N. Singh, R. M. Mehra, A. Kapoor, and T. Soga, "ZnO based quantum dot sensitized solar cell using CdS quantum dots," *Journal of Renewable and Sustainable Energy*, vol. 4, no. 1, Article ID 013110, 2012.

[7] M. Navaneethan, J. Archana, M. Arivanandhan, and Y. Hayakawa, "Functional properties of amine-passivated ZnO nanostructures and dye-sensitized solar cell characteristics," *Chemical Engineering Journal*, vol. 213, pp. 70–77, 2012.

[8] G. C. Yi, T. Yatsui, and M. Ohtsu, "ZnO nanorods and their heterostructures for electrical and optical nanode-vice applications," *Comprehensive Nanoscience and Technology: Nanomaterials*, vol. 1, pp. 335–374, 2011.

[9] C. Ma, Z. Zhou, H. Wei, Z. Yang, Z. Wang, and Y. Zhang, "Rapid large-scale preparation of zno nanowires for photocatalytic application," *Nanoscale Research Letters*, vol. 6, article 536, 5 pages, 2011.

[10] Z. Han, L. Liao, Y. Wu, H. Pan, S. Shen, and J. Chen, "Synthesis and photocatalytic application of oriented hierarchical ZnO flower-rod architectures," *Journal of Hazardous Materials*, vol. 217-218, pp. 100–106, 2012.

[11] L. Sun, D. Zhao, Z. Song et al., "Gold nanoparticles modified ZnO nanorods with improved photocatalytic activity," *Journal of Colloid and Interface Science*, vol. 363, no. 1, pp. 175–181, 2011.

[12] Y. Zhang, M. K. Ram, E. K. Stefanakos, and D. Y. Goswami, "Synthesis, characterization, and applications of ZnO nanowires," *Journal of Nanomaterials*, vol. 2012, Article ID 624520, 22 pages, 2012.

[13] E. Darezereshki, M. Alizadeh, F. Bakhtiari, M. Schaffie, and M. Ranjbar, "A novel thermal decomposition method for the synthesis of ZnO nanoparticles from low concentration $ZnSO_4$ solutions," *Applied Clay Science*, vol. 54, no. 1, pp. 107–111, 2011.

[14] R.-C. Wang and C.-C. Tsai, "Efficient synthesis of ZnO nanoparticles, nanowalls, and nanowires by thermal decomposition of zinc acetate at a low temperature," *Applied Physics A*, vol. 94, no. 2, pp. 241–245, 2009.

[15] A. V. Ghule, K. Ghule, C.-Y. Chen et al., "In situ thermo-TOF-SIMS study of thermal decomposition of zinc acetate dihydrate," *Journal of Mass Spectrometry*, vol. 39, no. 10, pp. 1202–1208, 2004.

[16] S. Labuayai, V. Promarak, and S. Maensiri, "Synthesis and optical properties of nanocrystalline ZnO powders prepared by a direct thermal decomposition route," *Applied Physics A*, vol. 94, no. 4, pp. 755–761, 2009.

[17] C.-C. Lin, W.-H. Lin, and Y.-Y. Li, "Field emission properties of ZnO nanowires synthesized by thermal decomposition process," *Journal of Physics D: Applied Physics*, vol. 41, no. 22, Article ID 225411, 2008.

[18] C.-C. Lin and Y.-Y. Li, "Synthesis of ZnO nanowires by thermal decomposition of zinc acetate dihydrate," *Materials Chemistry and Physics*, vol. 113, no. 1, pp. 334–337, 2009.

[19] X. Su, Z. Zhang, Y. Wang, and M. Zhu, "Synthesis and photoluminescence of aligned ZnO nanorods by thermal decomposition of zinc acetate at a substrate temperature of ~250°C," *Journal of Physics D: Applied Physics*, vol. 38, no. 21, pp. 3934–3937, 2005.

[20] H. Morkos and U. Ozgur, *Zinc Oxide Fundamentals, Materials and Device Technology, Alemania*, Wiley-VCH, Alemania, Germany, 2009.

[21] B. Madavali, H. S. Kim, and S. J. Hong, "Thermally decomposition of high quality ower-like ZnO nanorods from zinc acetate dihydrate," *Materials Letters*, vol. 132, pp. 342–345, 2014.

[22] M. Farbod and E. Jafarpoor, "Hydrothermal synthesis of different colors and morphologies of ZnO nanostructures and comparison of their photocatalytic properties," *Ceramics International*, vol. 40, pp. 6605–6610, 2014.

[23] N. Shakti, A. Prakash, T. Mandal, and M. Katiyar, "Processing temperature depe ndent morphological and optical properties of ZnO nanorods," *Materials Science in Semiconductor Processing*, vol. 20, pp. 55–60, 2014.

[24] R. Saravanan, E. Thirumal, V. K. Gupta, V. Narayanan, and A. Stephen, "The photocatalytic activity of ZnO prepared by simple thermal decomposition method at various temperatures," *Journal of Molecular Liquids*, vol. 177, pp. 394–401, 2013.

[25] M. S. Soosen, K. Jiji, C. Anoop, and K. C. George, "Optical phonon confinement in ZnO nanorods and nanotubes," *Indian Journal of Pure and Applied Physics*, vol. 48, no. 10, pp. 703–708, 2010.

[26] D. H. Zhang, Z. Y. Xue, and Q. P. Wang, "The mechanisms of blue emission from ZnO films deposited on glass substrate by r.f. magnetron sputtering," *Journal of Physics D: Applied Physics*, vol. 35, no. 21, pp. 2837–2840, 2002.

[27] S. Musić, D. Dragčević, S. Popović, and M. Ivanda, "Precipitation of ZnO particles and their properties," *Materials Letters*, vol. 59, no. 19-20, pp. 2388–2393, 2005.

[28] H. K. Yadav, K. Sreenivas, V. Gupta, J. F. Scott, and R. S. Katiyar, "Raman spectroscopy and dielectric studies of multiple phase transitions in ZnO:Ni," *Applied Physics Letters*, vol. 92, Article ID 122908, 2008.

[29] P. Kanti Samanta and A. Kumar Bandyopadhyay, "Chemical growth of hexagonal zinc oxide nanorods and their optical properties," *Applied Nanoscience*, vol. 2, pp. 111–117, 2012.

[30] K. J. Chen, T. H. Fang, F. Y. Hung et al., "The crystallization and physical properties of Al-doped ZnO nanoparticles," *Applied Surface Science*, vol. 254, no. 18, pp. 5791–5795, 2008.

[31] U. Pal, J. G. Serrano, P. Santiago, G. Xiong, K. B. Ucer, and R. T. Williams, "Synthesis and optical properties of ZnO nanostructures with different morphologies," *Optical Materials*, vol. 29, no. 1, pp. 65–69, 2006.

[32] A. K. Zak, M. E. Abrishami, W. H. A. Majid, R. Yousefi, and S. M. Hosseini, "Effects of annealing temperature on some structural and optical properties of ZnO nanoparticles prepared by a modified sol-gel combustion method," *Ceramics International*, vol. 37, no. 1, pp. 393–398, 2011.